Boundary-Layer Meteorol (2010) 136:301–324
DOI 10.1007/s10546-010-9502-3

ARTICLE

Improving the Mellor–Yamada–Janjić Parameterization for wind conditions in the marine planetary boundary layer

Kay Sušelj · Abha Sood

Received: 19 November 2008 / Accepted: 26 April 2010 / Published online: 16 May 2010

Abstract The structure of the lower part of the marine planetary boundary-layer (PBL) is relevant not only for climate and numerical weather prediction simulations but also for commercial applications such as offshore wind energy harvesting. A proper description of turbulence might have an important influence on the wind field properties such as the mean wind speed, turbulent fluxes and especially the vertical wind profile. In this study, the Mellor–Yamada–Janjić boundary-layer and surface-layer parameterizations in the Weather Research and Forecasting Model (WRF) were improved by redefining the master length scale (MLS), which controls the diffusion and dissipation of the turbulent fluxes as well as the pressure–temperature and pressure–strain covariances. In the surface layer, the modified MLS is dependent on the surface stability. In the PBL, the surface stability correction of the MLS is included, which has the strongest influence close to the surface. The non-local effects in the stable boundary layer based on surface heat forcing are also included. WRF model simulations with the original and the new PBL parameterization were compared with measurements. Improvements in the wind-shear simulations in the lower part of the boundary layer (up to around 30 m) with the new parameterization have been found, while its impact higher in the PBL is less pronounced. The simulated wind speed is however only slightly dependent on the boundary layer parameterization.

Keywords Marine boundary layer · Master length scale · Mellor–Yamada–Janjić scheme · Turbulence closure

K. Sušelj · A. Sood
ForWind, Carl von Ossietzky, University of Oldenburg, Oldenburg, Germany

Present Address:
K. Sušelj (✉)
Jet Propulsion Laboratory, California Institute of Technology, Pasadena, CA, USA
e-mail: kay.suselj@jpl.nasa.gov

Present Address:
A. Sood
National Institute of Water and Atmospheric Research Ltd., Wellington, New Zealand

1 Introduction

Enhanced turbulence in the planetary boundary layer (PBL) influences atmospheric mesoscale dynamics by increased vertical mixing. This effect is not explicitly resolved in mesoscale models but is parameterized by so-called closure models based on quantities resolved by the mesoscale model. For some applications, such as wind energy, pollution studies, air traffic, etc., where the near-surface atmospheric conditions are crucial, the choice of PBL parameterization in the mesoscale model becomes critical.

Turbulence parameterizations of different complexities have been proposed in the literature. Examples of a simple first-order closure model are described by Hong and Pan (1996), and a family of popular models, based on higher order closures, were introduced by Mellor and Yamada (1974) and further developed by Mellor and Yamada (1982); thus they are referred to as the Mellor–Yamada (MY) models. MY models were successively simplified by neglecting the highest orders of the turbulent anisotropy terms reducing the number of prognostic equations to be solved and are named according to the level of anisotropy that they describe. For example, the widely used MY level-2.5 model retains only the prognostic equation for the turbulent kinetic energy (TKE; trace of the turbulent stress tensor), while equations for other components of the turbulent stress tensor, the velocity–temperature covariances and temperature variance are simplified to algebraic equations. The even more simplified level-2 model without any prognostic equation can be used to provide the lower boundary conditions for any higher order MY model.

Three main weaknesses of the original MY models have been identified (e.g. Moeng and Wyngaard 1989; Cheng et al. 2002): (1) low order of the pressure–strain and pressure–temperature covariance closure, (2) down-gradient closure of the turbulent fluxes, and (3) the uncertainty defining the master length scale (MLS) that controls the rate of turbulent diffusion and dissipation and is used for the closure of the pressure–strain and the pressure–temperature covariances. Different authors treated the above mentioned weaknesses separately. For example, Cheng et al. (2002) improved the original closure of the pressure–strain and pressure–temperature covariances by including higher order terms. Their improved MY scheme produced turbulent fluxes closer to measurements as well as to large-eddy simulations. Among others, Canuto et al. (2001) derived the closure assumptions for the turbulent fluxes that were not restricted to be down-gradient. They showed that with their closure, the modelled turbulent fluxes resemble the results of large-eddy simulations well.

Despite vast amounts of effort to find the most appropriate equation for the MLS, due to the absence of an appropriate physically based equation, it is defined merely on plausible assumptions. In the original MY models, the MLS was defined as a combination of the Prandtl mixing length with a limiting value close to the surface and a length scale depending on the TKE distribution in the vertical column of the boundary layer as a limiting value towards the top of the boundary layer (Mellor and Yamada 1982). Umlauf and Burchard (2003) derived a generic equation for the MLS applicable to a large range of turbulent flows, and showed that many of the well-known expressions for the MLS are special cases of the generic length scale. However their generic length scale is more of a theoretical value, since in its original form it cannot be implemented in PBL parameterization schemes. Therry and Lacarrére (1983) distinguished between the length scale controlling dissipation and diffusion and further included a counter-gradient term into the turbulent exchange coefficient for heat. They argued that with these improvements, they were able to model the turbulent fluxes more realistically in the unstable atmosphere. Lenderink and Holtslag (2004) proposed that the MLS in neutral and convective conditions can be calculated as a combination of two length scales where both are vertically integrated functions of the Richardson numbe. The

first length scale limits the total length scale at the surface and the second one at the top of the boundary layer. They showed that, with their MLS formulation, the predictions of the wind and temperature profiles agree well with measurements at Cabauw. Teixeira et al. (2004) and Teixeira and Cheinet (2004) defined the length scale as a function of the local TKE and argued that this approach is more physical and showed that with this length scale the boundary-layer structure can be well represented. Nakanishi (2001) adjusted the original MY level-3 model and stability correction of the Prandtl mixing length and corrected MLS for non-local effects in the statically stable boundary layer forced from the surface, improved the closure assumption of the pressure–strain and pressure–temperature covariance and retuned the MY parameters based on the large-eddy simulation results for a dry atmosphere.

In our study, the MLS implemented in the MY level-2.5 model in the boundary layer, and the MY level-2 in the surface layer as part of the Weather Research and Forecasting Model (WRF)–Advanced Research WRF (ARW), Version 2 (Skamarock et al. 2005) by Janjić (2002) (therefore MYJ model), was modified based on the approach of Nakanishi (2001). The objective of this approach was to obtain an improved wind profile in the lower part (a few 100 m above the surface) of the marine PBL for different stability conditions, where modifications of the PBL scheme are simple. The WRF with the original (control) and adjusted (new) parameterization was used for downscaling atmospheric conditions over the North Sea and the Baltic Sea. The improvements of the simulated wind conditions with the new approach are estimated by comparing the simulation results with the measurements in the lower part of the PBL.

The organization of the paper is as follows: in Sect. 2 and Appendix A, the original MYJ PBL parameterization is briefly sketched. The modification of the MLS is described and new surface-integrated stability functions required in the surface layer are derived. The measurements used for the validation of the new scheme are presented in Sect. 3. The skill of the new scheme to reproduce the observed structure of the PBL within the framework of WRF is tested by comparing simulated results with the measurements (Sect. 4) and compared to the original scheme for selected cases as well as evaluated for a longer time period. Finally, the conclusions and discussions are presented in Sect. 5.

2 Adjustment of Boundary-Layer and Surface-Layer Parameterizations in the WRF Model

2.1 Original MYJ Parameterization in the WRF Model

Since the MY model in the WRF model is based on second-order closures, assumptions for the third-order moments $\left(\overline{u_i' u_j' u_k'}, \overline{u_i' u_j' \theta_v'}\right.$ and $\left.\overline{u_i' \theta_v'^2}\right)$, dissipation rates $\left(\nu \overline{\frac{\partial u_i'}{\partial x_k} \frac{\partial u_j'}{\partial x_k}}\right.$ and $\left.\alpha \overline{\frac{\partial \theta_v'}{\partial x_k} \frac{\partial \theta_v'}{\partial x_k}}\right)$, pressure–strain $\left(\overline{\frac{p'}{\rho}\left(\frac{\partial u_i'}{\partial x_j} + \frac{\partial u_j'}{\partial x_i}\right)}\right)$ and pressure–temperature gradient $\left(\overline{\frac{p'}{\rho} \frac{\partial \theta_v'}{\partial x_i}}\right)$ covariances are required.[1] The third-order moments are parameterized as down-gradient fluxes, i.e. they are equal to the negative of the product of the gradients of the second-order moments and a diffusion length scale. The dissipation terms are proportional to the respective variance divided by a dissipation length scale. The pressure–strain covariances are closed following

[1] The prime represents the fluctuations from the Reynolds-averaged values, θ_v is the virtual potential temperature, α and ν are the kinetic heat conductivity and kinetic viscosity respectively. Other symbols have their usual representation.

the assumption of Rotta (1951), retaining two highest order terms, the so-called turbulence self-interaction (return-to-isotropy, slow part) and shear-turbulence interaction (rapid part) terms. The turbulence self-interaction term is assumed to be proportional to the TKE and the turbulent anisotropy measure and divided by the MLS. The pressure–temperature gradient covariances are closed similarly, as the self-interaction term of the pressure–strain closure. One of the main assumptions in the MY scheme is that all above-mentioned length scales are proportional to each other everywhere in the boundary layer, therefore a single MLS l is postulated that controls all length scales.

The MY models are simplified further by applying a so-called 'boundary-layer approximation' by successively neglecting the highest orders of turbulent anisotropy. In the actual boundary layer,[2] the MY level-2.5 model additionally modified by Janjić (2002) as briefly described in Appendix A is used in WRF, where a prognostic equation for TKE is retained, while the mixing coefficients are a function of the non-dimensional wind shear, vertical virtual potential temperature gradient and TKE. In the surface-layer,[3] the level-2 model may be used which simplifies the prognostic equation of TKE to an algebraic equation by assuming local balance between turbulence production, diffusion and dissipation and thus the turbulent mixing coefficients are a function of the Richardson flux number (R_f). Łobocki (1993) showed that the MY level-2 model is equivalent to the Monin-Obukhov similarity theory (MOST), if the surface integrated stability functions are defined accordingly. Since the surface-layer parameterization in the WRF model is defined in terms of MOST, the MYJ level-2 model may also be used to derive integrated stability functions. In the original WRF model, the integrated surface stability functions are based on Paulson (e.g. Chen et al. 1997) for unstable conditions and on Holtslag and de Bruin (1988) for stable conditions. In our study, the new integrated surface stability functions were derived to be consistent with MYJ level-2 model and the newly defined MLS. For completeness, the equations of the MYJ level-2 and level-2.5 MYJ model are presented in Appendix A, where the coupling between the atmospheric surface layer and surface is briefly described. In the framework of the MY model, humidity is considered as a passive quantity, which only influences the buoyancy of dry air. This is done simply by using virtual potential temperature instead of potential temperature. Phase changes are dealt within other schemes and affect the turbulence only indirectly through changes to the large-scale parameters (Janjić 2002).

In the original MYJ model, the MLS in the atmospheric surface layer is assumed to be equal to the Prandtl mixing length (e.g. Stull 1988):

$$l_S = kz \tag{1}$$

where $k \approx 0.4$ is the von Karman constant and z is height above the surface. Mellor and Yamada (1982) proposed the limiting value of MLS at the top of the boundary layer to be:

$$l_T = \alpha \frac{\int_0^{h_p} zq\,dz}{\int_0^{h_p} q\,dz}, \tag{2}$$

where $\alpha = 0.3$ is empirically determined, $q = \sqrt{\overline{u_i' u_i'}}$ and TKE equals $\frac{1}{2}q^2$. Integration in Eq. 2 is from the surface to the top of the boundary layer (h_p). Inside the PBL, MLS is a 'harmonic sum' of both length scales l_S and l_T, so that total MLS is strongly determined by the shortest length:

[2] Actual boundary layer is defined from the first model level to the top of the boundary layer.

[3] Surface layer is defined from the surface to the first model level.

$$\frac{1}{l} = \frac{1}{l_S} + \frac{1}{l_T}. \tag{3}$$

2.2 Modifications to the Original MYJ Scheme

2.2.1 Surface Layer

Prandtl mixing length (Eq. 1) is usually taken to be the relevant macroscopic MLS in the near-neutral atmospheric surface layer (e.g. Stull 1988). In the surface layer far from neutral, it is expected that stability plays a strong role in the rate of turbulent mixing and diffusion that can be captured by adjusting the Prandtl mixing length. In the stable surface layer, the vertical movements are suppressed since additional energy is required to overcome the environmental stability, which leads to an effective decrease in the MLS. In the unstable surface layer, buoyancy enhances turbulent vertical mixing and diffusion, causing an effective increase of the MLS. Clearly, the characteristics of the surface layer itself are stability dependent since the turbulent fluxes depend on stability (Appendix A). With a stability correction of the surface MLS the rate of the dissipation and diffusion is adjusted accordingly. Łobocki (1992) showed that the MY level-2 model with the Prandtl mixing length does not have the correct limits of the normalized fluxes with increasing or decreasing surface stability, and suggested that this issue can be resolved by defining a stability dependent MLS. Nakanishi (2001) suggested the surface MLS to be a function of the non-dimensional surface stability $\zeta = z/L$, where L is the Obukhov length and z is the height above the surface, viz.

$$l_S = kz(a + b\zeta)^c \tag{4}$$

where a, b and c are empirical constants and the Obukhov length (L) is defined as:

$$L \equiv -\frac{u_*^3 \theta_v}{kg\overline{w'\theta_v'}} \tag{5}$$

with the friction velocity $u_* \equiv (\overline{u'w'}^2 + \overline{v'w'}^2)^{1/4}$. Nakanishi (2001) performed a set of idealized large-eddy simulations (LES), and by applying the assumptions of the MY level-2 models, he fitted the surface MLS to LES results. For the stable layer ($\zeta > 0$), the best fit with parameters $a = 1$, $b = 2.7$ and $c = -1$ from Eq. 4 was obtained. In the unstable layer ($\zeta < 0$), he used the original Prandtl mixing length (i.e. $c = 0$ in Eq. 4) and changed the l_S only in the actual boundary layer using parameters: $a = 1, b = -100$ and $c = 0.2$. Our experiments showed that increasing the surface MLS in the unstable surface layer improves the agreement between the simulations and measurements. The surface MLS used herein is defined as:

$$l_S = \begin{cases} kz(1 + 2.7\zeta)^{-1} & \zeta > 0 \\ kz & \zeta = 0 \\ kz(1 - 100\zeta)^{0.2} & \zeta < 0 \end{cases} \tag{6}$$

In the very stable surface-layer ($\zeta \to \infty$), the MLS should become independent of height (Łobocki 1992), since the turbulence becomes decoupled from the surface and height is in this case irrelevant as a turbulent surface scaling parameter. The new definition of the MLS agrees with these limiting values ($l \to kL/2.7$ when $\zeta \to \infty$). In the very unstable surface layer ($\zeta \to -\infty$), the MLS should be proportional to z. The newly defined MLS does not exactly fulfil this requirement since $l \propto z^{1.2}$ when $\zeta \to -\infty$. However, this is not a serious limitation, since Janjić (2002) imposed the upper limit on MLS in the actual boundary layer to avoid numerical instabilities of the scheme.

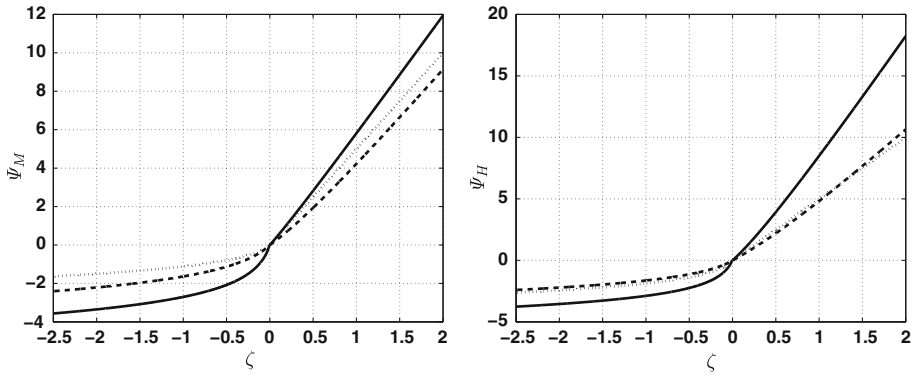

Fig. 1 Integrated stability functions for momentum (Ψ_M, *left*) and heat (Ψ_H, *right*). The *dotted lines* represent the original WRF model, *dashed* Łobocki (1993) (MY level-2 with Prandtl mixing length) and *solid lines* new stability functions

The integrated stability functions for momentum and heat ($\Psi_M(\zeta)$ and $\Psi_H(\zeta)$, respectively)[4] defined within the framework of MOST are required in order to relate the surface values of temperature, momentum and moisture to the values at the first model level. Here, the integrated stability functions are derived from the MY level-2 model with the surface length scale as defined in Eq. 6. The turbulent mixing in the MY level-2 scheme is expressed as a function of the flux Richardson number (R_f), while the integrated stability functions are functions of the surface stability parameter ζ. The implicit relation between R_f and ζ from the level-2 MY equation is derived by Łobocki (1993, Eq. A31):

$$\frac{l_S}{kz} = \frac{R_f(1-R_f)^{-1/4}}{S_M^{3/4} B_1^{1/4} \zeta} \tag{7}$$

where S_M is the non-dimensional diffusion coefficient for momentum and B_1 is a constant of the level-2 MY model (for details see Appendix A). From the definitions of the integral stability functions (Ψ_M and Ψ_H), the flux Richardson number (R_f) and the gradient Richardson number (R_i), the integrated stability functions are expressed as (Łobocki 1993):

$$\Psi_M(\zeta) \equiv \int_0^\zeta \frac{\phi_M(\zeta')-1}{\zeta'} d\zeta' = \int_0^\zeta \left(\frac{1}{R_f} - \frac{1}{\zeta'}\right) d\zeta', \tag{8}$$

$$\Psi_H(\zeta) \equiv \int_0^\zeta \frac{\phi_H(\zeta')-1}{\zeta'} d\zeta' = \int_0^\zeta \left(\frac{R_i}{R_f^2} - \frac{1}{\zeta'}\right) d\zeta', \tag{9}$$

where ϕ_M and ϕ_H are the stability functions defined within MOST. The ratio of the gradient and flux Richardson numbers (R_i/R_f) in Eq. 9 can be expressed as a ratio of the non-dimensional diffusion coefficients for momentum and heat ($S_M(R_f)$ and $S_H(R_f)$, respectively) and is a function of ζ. The integrated stability functions are obtained by numerically integrating Eqs. 8 and 9.

In Fig. 1, the following integrated stability functions are shown: (1) from the original WRF model, (2) derived by Łobocki (1993) (from the MY level-2 model where the Prandtl mixing length is used as the MLS), and (3) derived similarly as in Łobocki (1993), but with the MLS

[4] The integrated stability function for heat is also used for moisture and other passive scalars.

from Eq. 6. Both the integrated stability functions for heat and momentum implemented in the original WRF model and the one from Łobocki (1993) differ only slightly, while the new stability functions are considerably different. In the unstable surface layer ($\zeta < 0$), the new stability functions for momentum (heat) are lower than the other two, which implies that the parameterization with new stability functions will yield weaker vertical wind shear (virtual potential temperature and moisture gradients). In the stable surface layer ($\zeta > 0$), it is the opposite; the new stability functions for momentum (heat) are considerably higher than the other two, which implies that the parameterization with the new stability functions will yield higher vertical wind shear (virtual potential temperature and moisture gradients).

The numerical fitting of the new integrated stability functions to ζ leads to the following relationships:

$$\Psi_M(\zeta) = \begin{cases} \dfrac{\zeta}{R_{fc}} + 1.1223\exp(1 - 1.6666/\zeta) & \zeta > 0 \\ -0.9904\ln(1 - 14.264\zeta) & \zeta \le 0 \end{cases}, \tag{10}$$

$$\Psi_H(\zeta) = \begin{cases} \dfrac{\zeta R_{ic}}{R_{fc}^2 \Phi_T(0)} + 8.209\zeta^{1.1091} & \zeta > 0 \\ -1.0103\ln(1 - 16.3066\zeta) & \zeta \le 0 \end{cases}, \tag{11}$$

where the values for the critical Richardson number $R_{ic} = 0.183$ and critical flux Richardson number $R_{fc} = 0.19$ and the ratio between gradient and flux Richardson number in the neutral atmosphere $\Phi_T(0) = 0.8$ were used.

2.2.2 Boundary-Layer

The MLS in the actual boundary layer was taken from Nakanishi (2001). He defined the inverse of the MLS as the sum of the inverses of three different length scales: the surface-layer length scale (l_S), the length scale related to the turbulence property of the PBL (l_T) and the buoyancy suppression length scale (l_B). Formally, the MLS is written as:

$$\frac{1}{l} = \frac{1}{l_S} + \frac{1}{l_B} + \frac{1}{l_T}, \tag{12}$$

where l_S is defined in Eq. 6 and l_T and l_B are:

$$l_T = \alpha_1 \frac{\int_0^{h_p} qz dz}{\int_0^{h_p} q dz}, \tag{13}$$

$$l_B = \begin{cases} \alpha_2 q/N & \partial\theta_v/\partial z > 0 \quad \text{and } \zeta \ge 0 \\ (\alpha_2 q + \alpha_3 q\sqrt{(q_c/l_T N)})/N & \partial\theta_v/\partial z > 0 \quad \text{and } \zeta < 0 \\ \infty & \partial\theta_v/\partial z \le 0 \end{cases}. \tag{14}$$

The surface length scale (l_S) is equal to the MLS in the surface layer and whose role is to constrain MLS close to the surface. The l_T is the same as in the original MY definition with a different constant $\alpha_1 = 0.23$. The role of the buoyancy length scale (l_B) is to constrain the MLS in a statically stable atmosphere, especially in the upper part of the boundary layer. Here N is the Brunt–Väisälä frequency and q_c is the vertical velocity scale defined as $q_c = (g/\theta_{vs}\overline{w'\theta_v'}|_s l_T)^{1/3}$, where the subscript s indicates values at the surface. The parameters in Eq. 14 were set to $\alpha_2 = 1$ and $\alpha_3 = 5$ based on LES results.

3 Experimental Data

The ability of the WRF model with the new and control parameterizations to reproduce the observed near-surface wind conditions in the lower part of the PBL is investigated by comparing the WRF simulation with wind measurements at two measuring field stations: (1) the Östergarnsholm tower operated by the University of Uppsala (Sweden) located in the Baltic Sea outside Gotland which measures wind speed and temperature up to around 30 m above mean sea level (m.s.l.), and (2) the FINO tower in the North Sea, where measurements are performed between 30 and 100 m above m.s.l.

3.1 Observations at Östergarnsholm

The field station Östergarnsholm is situated 4 km east of Gotland in the Baltic Sea (lat. 57°26′ N, lon. 18°54′ E). The wind measurements at Östergarnsholm tower are available at levels 1–5 at heights of 7.9, 12.8, 15.3, 21.2 and 29.8 m above m.s.l., respectively. The variation in the measurement height due to the influence of the tide, the order of 0.5 m, is neglected. The heat and momentum fluxes are derived from the high resolution (20 Hz) sonic wind speed and virtual temperature measurements 9 m above m.s.l. The turbulent fluxes provided by the University of Uppsala (Rutgersson et al. 2001) were calculated from the deviations of wind speed and temperature from the 10- min running mean average and then averaged over an hour. Only the measurements representing open sea conditions and where the wind speed is not influenced by the tower structure (wind direction between 80° and 220°) are used. More details on the flux calculations and the applied corrections can be found in Smedman et al. (1999). Due to the dynamical influence of the waves on the PBL structure (Sjöblom and Smedman 2003), which is not properly described in the WRF model, but influences the wind profile close to the interface between atmosphere and sea (Rutgersson et al. 2001), only measurements from the upper instrument levels were used (3rd–5th). Sjöblom and Smedman (2003) showed that the wind profiles between these measuring levels are not much influenced by wave effects, while the wind profiles at the lower measuring heights are sensitive to the wave conditions.

3.2 Observations at FINO

The FINO research platform (Neumann et al. 2004) located in the North Sea (lat. 54°0.86′ N, lon. 6°35.26′ E) performs multilevel measurements of three-dimensional velocity and temperature with sonic instruments (10 Hz temporal resolution) as well as with the lower resolution (1 Hz) cup anemometers, which were used here only for correction of the sonic data. The sonic and cup instruments are positioned at the opposite tower arms enabling correction of the tower-wake effects on wind measurements. For our study, the wind speeds at 40 m, 60 m and 80 m above m.s.l. were used to derive the wind shear. The turbulent momentum and heat fluxes were calculated from the measurements at 40 m to represent the surface conditions. After calibration, quality control and peak removal from the sonic time series with a method similar to Vickers and Mahrt (1997), the influence of the anemometer tilt on the vertical wind speed has been corrected using a planar fit method described by Wilczak et al. (2001). The influence of the tower wake on the horizontal wind speed has been corrected using the cup anemometer measurements. The data at the wind shadow of the tower structure with wind directions between 90° and 170° were disregarded. More details of the FINO corrections can be found in Sušelj (2009). The turbulent fluxes were calculated from the wind speed and

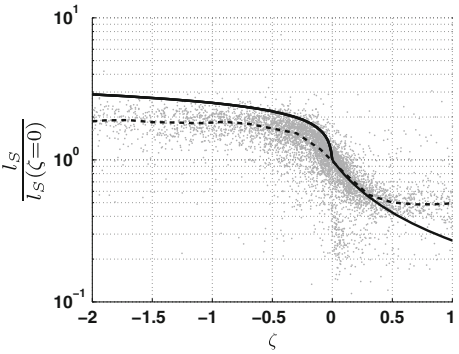

Fig. 2 Scatterplot of the integral length scale normalized by its near-neutral value as a function of stability (ζ) from the FINO data. *Solid line* new normalized MLS, *dashed line* median from FINO measurements

virtual temperature anomalies relative to the 20-min running mean values. The sensitivity study showed that the fluxes were not overly sensitive to the averaging time used (not shown).

From the high resolution wind measurements at FINO, the surface MLS (l_S) can be estimated as a vertical integral length scale as done by Iwata et al. (2009), under the following assumptions. The turbulent eddies with the largest vertical scale in boundary-layer flow are the most efficient in turbulent diffusion and dissipation. The vertical size of the largest eddies is estimated as the height difference at which the autocorrelation of the vertical wind speed falls to e^{-1}. To estimate the vertical size of eddies, the correlation of the 20-min segments, linearly detrended vertical wind speed between the three different measuring levels, is calculated and assumed to be a function of the distance between the corresponding measurement levels. To obtain l_S, the exponential function is fitted to the correlation function:

$$\frac{1}{\sigma_{w'(r)}\sigma_{w'(r+\Delta r)}} \int w'(r,t)w'(r+\Delta r,t)dt = e^{-\Delta r/l_S} \tag{15}$$

where σ is the standard deviation of the corresponding field.

In Fig. 2, the l_S normalized by its near-neutral value (i.e. the mean value for $|\zeta| < 0.15$) calculated from FINO data and that from the new parameterization is plotted against the stability parameter ζ.[5] Although the scatter of the l_S from FINO is considerable, the clear dependence of l_S on ζ can be seen, with decreasing (increasing) l_S in the stable (unstable) surface layer. The l_S from measurements and that used in the WRF model show a similar dependence upon stability.

4 Results

The WRF model was used to refine the state of the atmosphere, especially the boundary layer, by downscaling the global NCEP Final Analysis (FNL).[6] The non-hydrostatic version of the model with Ferrier microphysics, rapid radiative transfer in the longwave, the Dudhia shortwave scheme and Betts–Miller–Janjić convective (not used in the third domain; look below for the explanation of the domain) scheme was used. Over the land, the NOAH surface scheme was selected, while the viscous sublayer was implemented over the sea. More details of the model and references can be found in Skamarock et al. (2005).

[5] Note that the normalized l_S from the original WRF is independent on stability.

[6] Available at: http://dss.ucar.edu/datasets/ds083.2/

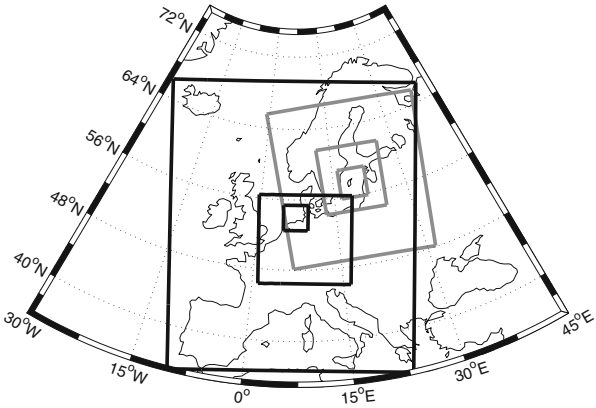

Fig. 3 WRF simulation domains. The *black boxes* indicate the FINO simulation domains and *grey boxes* the domains for the Östergarnsholm simulations

Two sets of simulations were performed: (1) the *control* simulation (WRF with original MJY boundary-layer and surface-layer parameterizations), and (2) the *new* simulation (WRF with parameterizations as described in this paper) to investigate whether the representation of the vertical structure of the wind speed in the lower part of the boundary layer is improved. Separate simulations for each measuring location (Fig. 3) were performed, where three (two-way) nested domains were defined with horizontal resolution of 27, 9 and 3 km, respectively. In the vertical, 35 η levels were set, typically four half-levels (on which the horizontal wind speed is calculated) were below 100 m and the first half-level is at around 8 m above the surface. The WRF model was initialized every second day at 1800 UTC from FNL data with a horizontal resolution of $1^\circ \times 1^\circ$, discarding the first 6 h as spin-up and retaining the subsequent hourly data for 48 h starting at 0000 UTC in the time series. The lateral boundary conditions of the first domain were updated every 6 h from the FNL analysis. The boundary-layer structure is very sensitive to the sea-surface temperature (SST), since the difference between SST and the temperature of the overlying air is related to the surface-layer stability. In the Baltic Sea, the SST, being highly variable in space, cannot be properly described by the relatively low resolution FNL data. Therefore, for the simulations at Östergarnsholm , the 3-day averaged high resolution ($\approx 1 \times 1$ km) analysis of satellite measured SST, provided by the German Federal Maritime and Hydrographic Agency (Bundesamt für Seeschifffahrt und Hydrographie, BSH) was used instead. For the simulations at FINO the SST from FNL was used, since its spatial variability is well captured. The SST field was however kept constant throughout the simulation period.

The WRF results were bi-linearly interpolated in the horizontal from the nearest four points to the location of the measurement tower. The wind speed was linearly interpolated in the vertical from the model half-levels to the measurement heights. The comparison of the measurements with the simulation data is shown first for the selected cases (Sect. 4.1) and then for the complete period (Sect. 4.2).

4.1 Case Studies

The structure of the boundary layer over the sea is different from the boundary layer over the land in many respects. Over land, the PBL dynamics have typically a pronounced diurnal

cycle resulting primarily from the surface diabatic heating and cooling. Over the sea, the PBL structure is mainly determined by the properties of advected air masses and has little or almost no diurnal cycle. At FINO, especially in the winter, the south-westerlies to westerlies advect warmer air over a cold sea, which results in a stable boundary layer, while north-westerlies to north-easterlies advect cold air and the resulting boundary layer is unstable. Although less clear, a similar relationship between stability and the large-scale flow is observed at Östergarnsholm .

Therefore, the conditions over the sea allow an investigation of the structure of the PBL with the same stability conditions persisting over a number of days. In the case studies, we investigated how the vertical wind shear is represented by both control and new PBL parameterizations. The case of the unstable surface layer at FINO was not shown, since only small differences between the new and the control parameterizations are found.

4.1.1 Stable Case at Östergarnsholm

For the representative case of the stable surface layer at Östergarnsholm , the period from 3 November 2005 at 0000 UTC to 5 November 2005 at 0000 UTC was selected. The synoptic situation over the Baltic Sea was determined by a low pressure system over the Atlantic and north-western Europe and a high pressure system above the south-eastern and eastern Europe, which did not change significantly during this period. Near-surface winds over the Baltic Sea were southerly advecting warm air over the Baltic Sea. At Östergarnsholm , the difference between the SST and the near-surface air temperature was around 2 K, which resulted in the formation of a stable surface layer and a surface inversion persisting throughout the study period.

The wind speed at the fifth measurement level at Östergarnsholm increased from about 7 m s^{-1}at the beginning of the period to about 12 m s^{-1}in the evening of 3 November and decreased to 9 m s^{-1}towards the end of the period. The results from the control simulation as well as from the new simulation underestimate wind speed by about 1 m s^{-1}(Fig. 4a). The wind speed does not show a sensitivity on the selection of the PBL parameterization. The magnitude of the heat flux is overestimated in both model versions compared to the measurements (Fig. 4b). As shown further, the magnitude of the heat flux is overestimated in virtually all simulation results. The reason for that is not clear, but the following is plausible: (1) the heat flux has a high sensitivity to the temperature difference between the air and the sea surface together with imprecise specification of the SST, (2) the parameterization of the surface diffusive layer is inadequate, or (3) the parameterization of the boundary layer itself is inadequate. In this case study, the temperature of the air as well as SST agreed well (within 0.5 K) with the measurements. The simulated friction velocity reproduces measurements well, not differing much between the control and new version (Fig. 4c). An interesting result of this case study and for almost all case studies shown here is that the turbulent fluxes computed from the control and new parameterizations are almost the same. Further one-dimensional (only vertical) model investigations (Sušelj 2009) indicated that in the stable (unstable) atmosphere the new parameterization yields lower (higher) values of exchange coefficients that are compensated by the higher (lower) vertical gradients of the wind speed and potential temperature. Since in the MYJ model the turbulent fluxes are the product of the vertical gradients and the exchange coefficients, the resultant turbulent fluxes between the new and control simulations do not change significantly.

The results of the control simulations show that the model underestimates the wind shear between the upper Östergarnsholm measuring levels (Fig. 4e–f), which is well corrected by the results of the new simulation. Also the vertical profile of the time-averaged wind speed

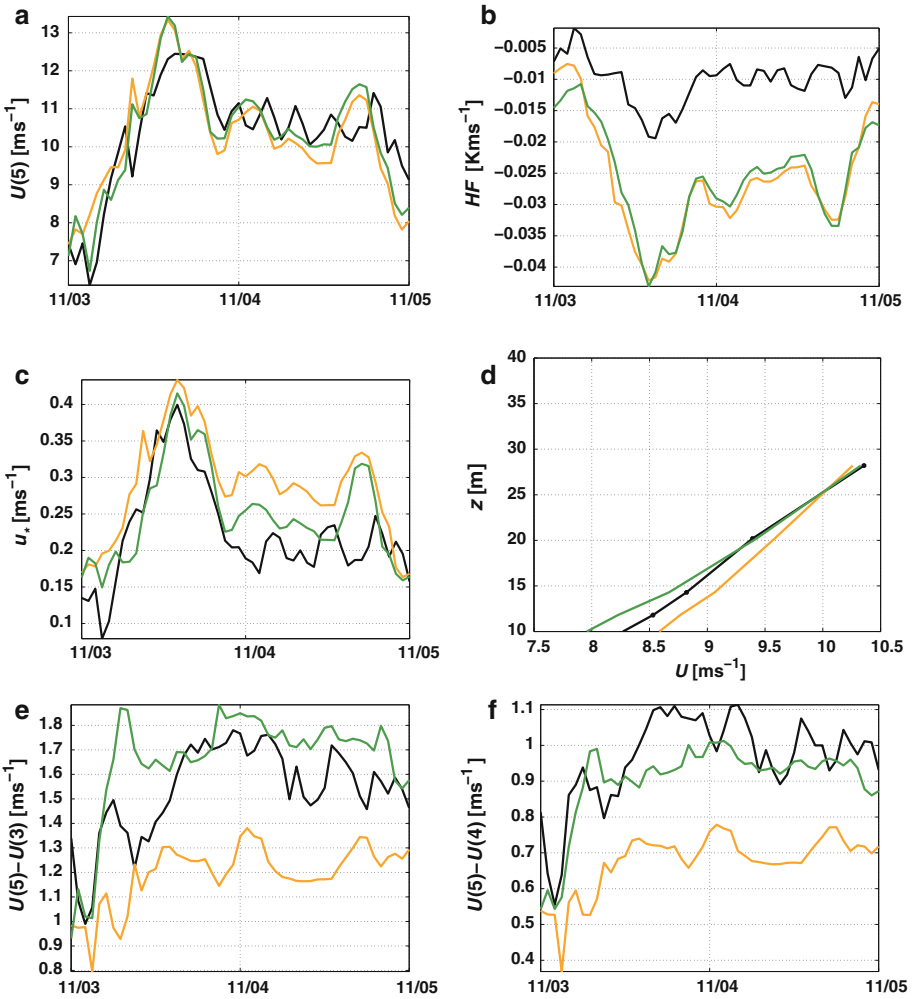

Fig. 4 Stable case at Östergarnsholm . **a** Wind speed at level 5; **b** surface heat flux; **c** surface friction velocity; **d** time-averaged wind profile; **e** wind speed difference between level 5 and 3; **f** wind speed difference between level 5 and 4. Measurements (*black*) new WRF (*green*) and control WRF (*yellow*) are shown

(Fig. 4d) from measurements agrees much better with the results of the new simulation than to those of the control run, except for wind shear very close to the surface. As already discussed, the probable reason for the disagreement between measured and simulated wind shear at the first few measuring levels is the dynamical influence of the waves on the boundary-layer structure, which is not considered adequately in the WRF model.

4.1.2 Stable Case at FINO

The case from 16 March 2005 at 0000 UTC to 18 March 2005 at 1200 UTC was chosen as a case representing stable surface conditions at FINO. The synoptic situation during this period is similar to the one defining the stable surface condition at Östergarnsholm with a

low-pressure system over the Atlantic and a high-pressure system over southern Europe. During the simulation period, the high-pressure system shifts to the north-west. At the beginning of the period, near-surface south-westerlies dominate over the North Sea, which later turn towards the north-west. The wind advects warm air from western Europe over a cold sea. The wind speed is around 17 m s^{-1} at the beginning of the period decreasing to 13 m s^{-1} in the night of 16–17 March and is relatively well simulated by both model versions (Fig. 5a). The temperature differences between the near-surface air and the sea at the beginning of the simulation is about 3 K. The magnitude of the surface heat flux is even higher than at Östergarnsholm (Fig. 5b), which is primarily due to a higher temperature difference between the sea and the overlying air. As with the stable case at Östergarnsholm , the heat flux is overestimated by both control and new simulation results. In this case, the friction velocity seems

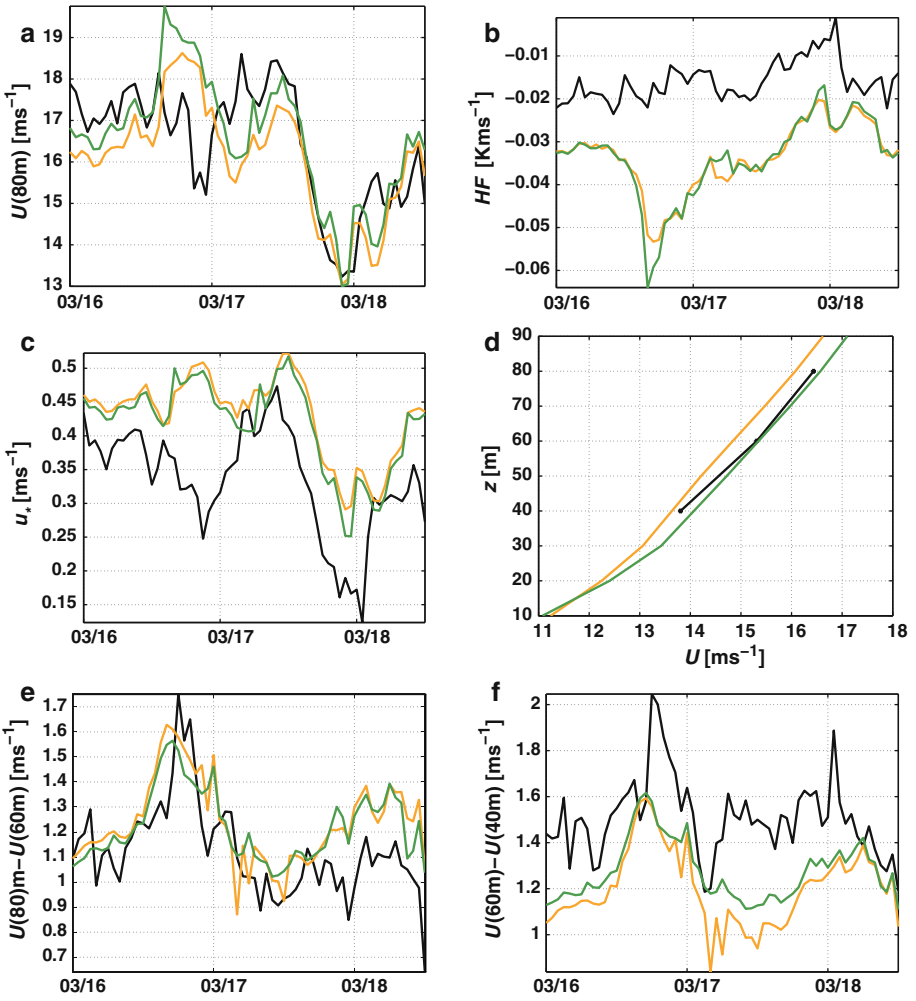

Fig. 5 Stable case at FINO. **a** wind speed at 80 m height; **b** surface heat flux; **c** surface friction velocity; **d** time-averaged wind profile; **e** wind speed difference between 80 and 60 m height; **f** wind speed difference between 60 and 40 m height. Measurements (*black*) new WRF (*green*) and control WRF (*yellow*) are shown

to be slightly overestimated by both versions (Fig. 5c), though inaccuracies in measurements cannot be eliminated. The measured friction velocity is estimated from the measurements at 40 m, which is expected to be lower than the real surface value (e.g. Gryning et al. 2007). Similar to the previous case study, the differences of turbulent fluxes between new and control simulations are only minor.

At the FINO measurement levels, the vertical wind shear between the control and the new parameterizations did not change considerably (Fig. 5d–f). The control parameterization is well able to reproduce the wind shear between the upper two levels (80 and 60 m), while at the lower two levels (60 and 40 m), it is slightly too low. With the new parameterization, the wind-speed difference between the lower two measurement levels is slightly higher, closer to the measurements, while between the upper two levels it remains almost unchanged. This case indicates that the corrections of the PBL parameterizations have an important effect only in the surface layer (below ≈40 m), while at the FINO levels, the differences between both WRF simulations are minor.

4.1.3 Unstable Case at Östergarnsholm

The case from 4 August 2005 at 0200–1200 UTC was chosen to represent unstable conditions at Östergarnsholm . The synoptic situation was characterized by an approximately zonal sea-level pressure gradient with a high-pressure system over south-western and western Europe and the Atlantic, and with a high-pressure system north of the Azores, and a low-pressure system over Iceland. The Baltic Sea was under a high-pressure system, and westerly near-surface wind transported colder air from the Atlantic to the Baltic Sea.

The comparison of measurements at Östergarnsholm with simulations is shown in Fig. 6. Almost no heat flux (nearly-neutral surface layer) is observed at the beginning and at the end of the period. The winds were weak throughout the whole period (between 4.5 and 7 m s^{-1} at the fifth level), which were slightly underestimated at the end of the period. The simulated friction velocity as well as the heat flux was overestimated compared to the measurements. The wind shear between the upper levels (3–5) in the control simulation results was overestimated, which was improved in the new simulation. The shape of the time-averaged wind profile from the measurements agrees significantly better with the new parameterization results than with the control parameterization results, even though the wind speed is underestimated in both cases.

4.2 Statistics

Analysis of the case studies shown in the previous subsection indicates the expected improvement of the new parameterization compared to the control parameterization. The wind speed itself is only slightly dependent on the PBL parameterization. The differences between new and control parameterizations are largest close to the surface (at Östergarnsholm measurement heights—below 30 m) while higher in the boundary layer (at FINO measurement heights between 40 and 80 m) they are smaller. Furthermore, the absolute values of the differences between the new and control parameterizations are higher for the stable case than for the unstable case. In this section, the improvement of the new PBL parameterization in the WRF model is investigated for the complete time period of the available measurement data (i.e. 7 months for Östergarnsholm and 12 months for FINO).

The wind speeds are almost equally well simulated by both versions at both measurement towers. The root-mean-square error (rmse) of the simulated wind speed between the

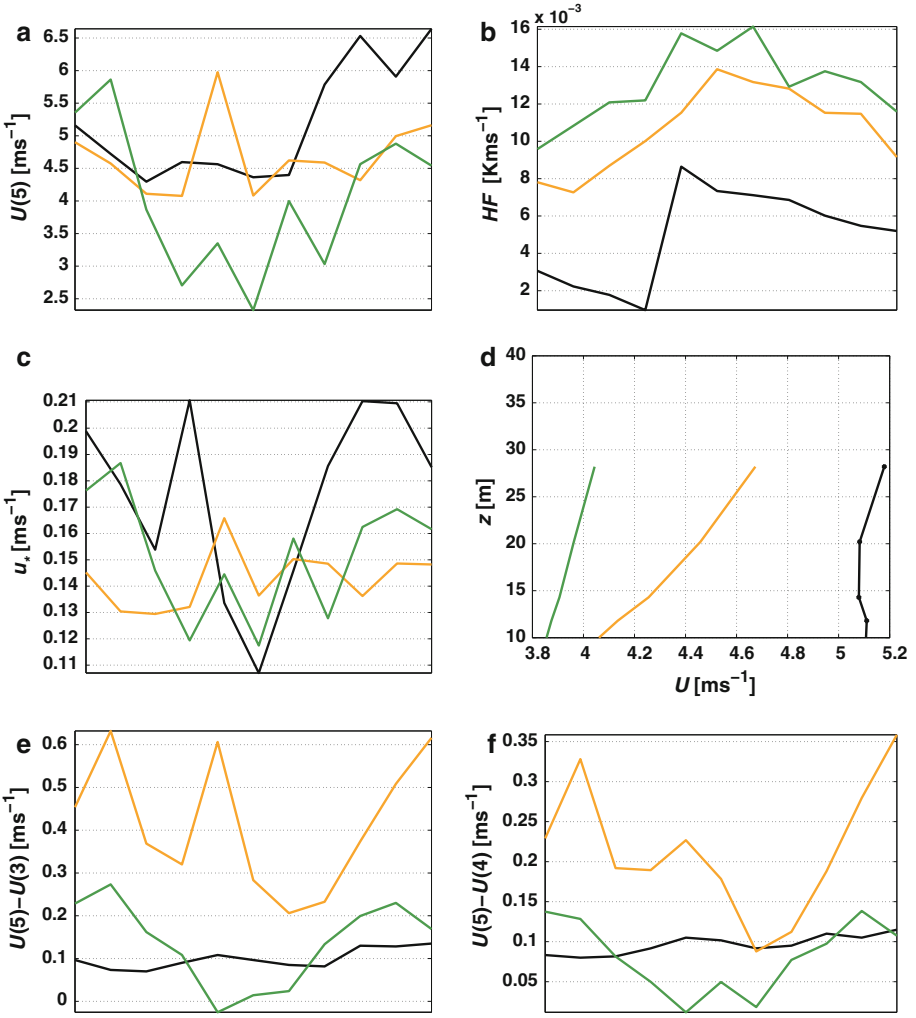

Fig. 6 Same as Fig. 4, only for unstable case

Table 1 Root-mean-square error (m s^{-1}) between wind speed measurements and WRF simulation results

Measurement	Level (m)	Control	New
FINO	40	2.10	2.14
FINO	60	2.25	2.30
FINO	80	2.31	2.36
Östergarnsholm	14.3	1.66	1.62
Östergarnsholm	20.2	1.66	1.63
Östergarnsholm	28.8	1.69	1.67

control and new parameterizations differs by less than 0.05 m s^{-1} (Table 1). Fig. 7 compares the measured and simulated wind speeds at the upper measurement levels, where it is confirmed again that the choice of the parameterization does not significantly influence the mean

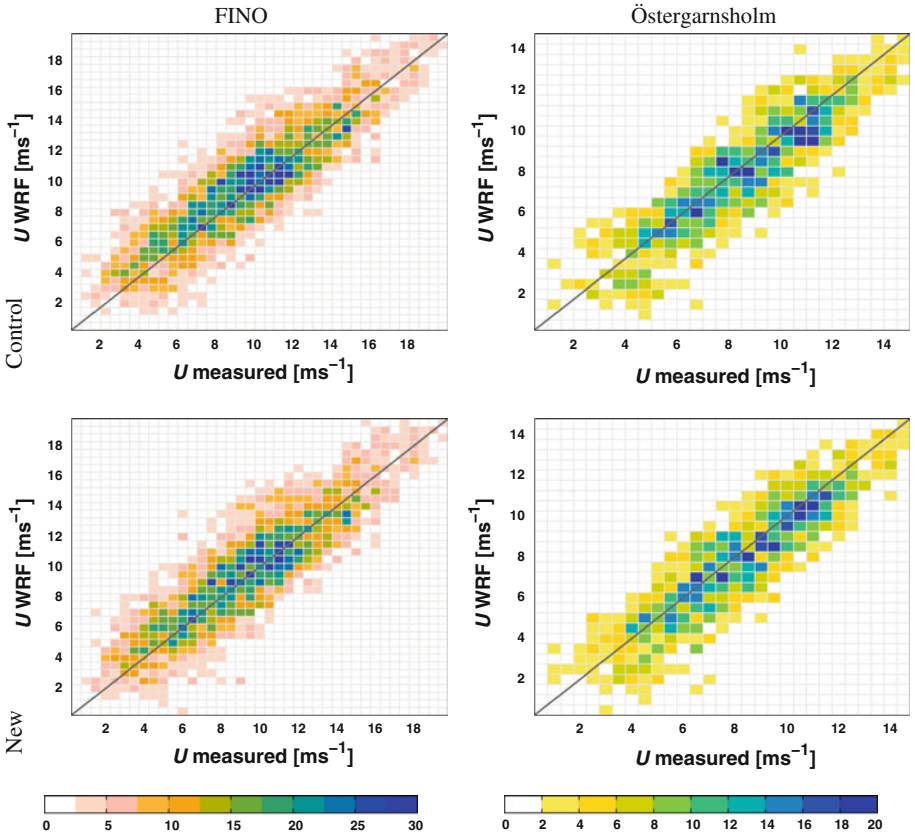

Fig. 7 Histogram of measured (x-axis) against simulated (y-axis) wind speeds. *Left* for the WRF model at 80 m height, *right* for Östergarnsholm and at level 5; *upper panel* for the control simulation and *lower* for the new simulation

horizontal wind speeds. It can also be seen from Fig. 7 that both the high and low wind speeds are equally well simulated.

Since lower boundary conditions, characterized by the surface friction velocity (u_*) and the inverse surface Obukhov length ($1/L$), are explicit terms controlling the wind profile in both parameterizations, they are compared in Figs. 8 and 9 respectively. At Östergarnsholm , the friction velocity in the control version agrees well with the measurements, although the scattering between the observations and the WRF simulation is considerable. The scattering can be partly related to the inadequate estimation of the friction velocity by the Charnock relationship. At FINO, the simulated friction velocity is on average higher than measured. A plausible reason may be that the friction velocity from FINO, which is obtained at 40 m above m.s.l., does not represent the surface conditions properly. The $1/L$ values obtained from the control simulation agree relatively well with the measured $1/L$ at both measurement platforms in the stable regime ($L > 0$), although there is a slight consistent underestimation of the stability (i.e. the measured $1/L$ is consistently higher than the observed values) (Fig. 9). In the unstable regime ($L < 0$), the simulations show consistently a more unstable atmosphere (again measured $1/L$ is consistently higher than the simulated one). The stability dependent difference of $1/L$ is mainly a consequence of too large a magnitude of the simulated heat

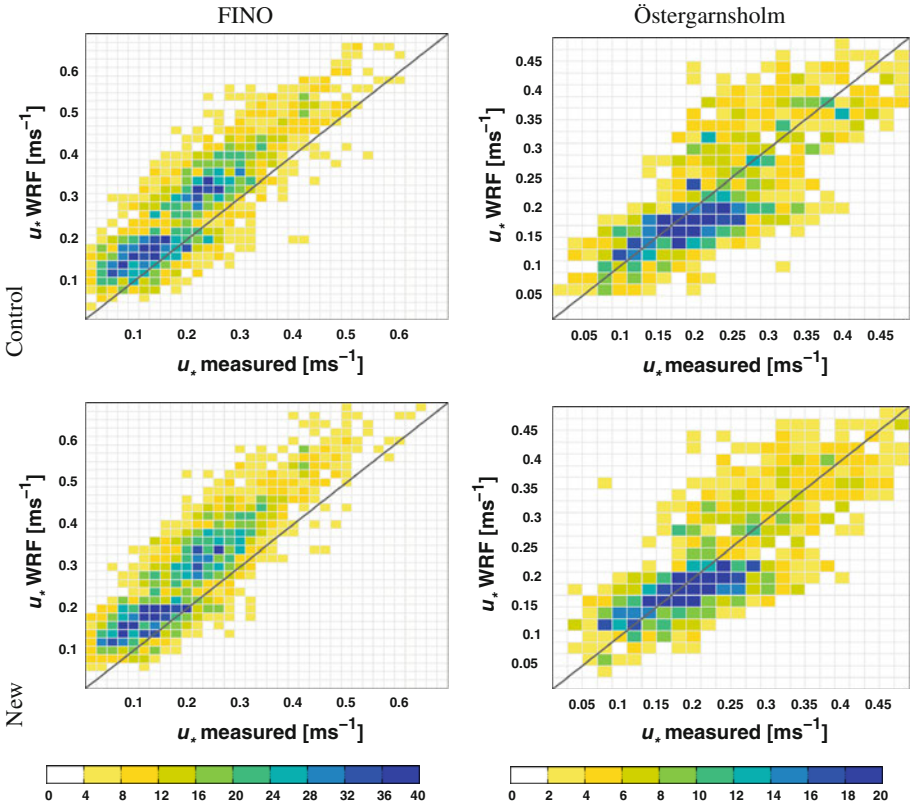

Fig. 8 Same as Fig. 7, only for surface u_*

flux (not shown). As in the case studies, improving the parameterization does not have a significant influence on the friction velocity and turbulent heat flux. The overestimation of the heat flux magnitude by the WRF model, which leads to the overestimation in the magnitude of $1/L$, can result in an overly strong correction of the MLS in the surface layer and thus an overly strong correction of wind profiles. The deviation of the heat flux is not necessarily a problem in the PBL parameterization, since it is strongly determined by the temperature difference between the lower part of the atmosphere and the sea surface as well as with the parameterization of the diffusive layer.

The comparison of the measured and simulated wind shear is shown in Table 2 (dependent on stability) and in Fig. 10. The improvement of the new parameterization at FINO levels is only marginal for all stability cases. Based on the case studies this is a reasonable result, since it was shown that the wind shear between the new and control parameterizations does not differ considerably at the FINO measurement levels (between 40 and 80 m). At Östergarnsholm , the improvement of the wind shear in the new parameterization is observed for all stability cases. In the stable cases (roughly, the high wind-shear region in Fig. 10), the wind shear from the control parameterization is too small, which is considerably improved with the new parameterization. For the unstable cases (the low wind-shear region in Fig. 10), the control parameterization yields wind shears that are too high, but which are decreased in the new parameterization. The improvement is also indicated by the smaller rmse of the wind-speed

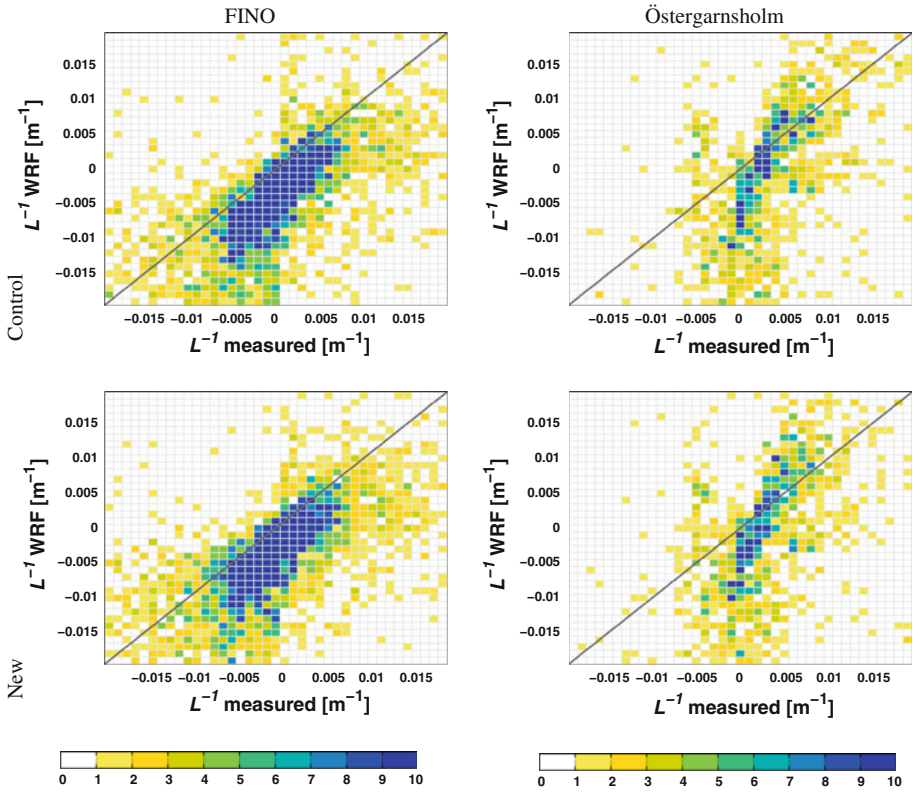

Fig. 9 Same as Fig. 7, only for surface $1/L$

Table 2 Root-mean-square error of wind shear ($100\,s^{-1}$) from the WRF model, for stable ($1/L > 0.005\,m^{-1}$), unstable ($1/L < -0.005\,m^{-1}$), neutral ($0.005\,m^{-1} < 1/L < 0.005\,m^{-1}$) and all conditions

	Stable	Unstable	Neutral	All
FINO between height of 80 and 40 m				
Control	3.07	1.17	1.50	1.84
New	3.06	1.07	1.47	1.79
FINO between height of 80 and 60 m				
Control	3.91	3.20	6.51	5.00
New	3.87	3.15	6.52	4.98
Östergarnsholm between levels 5 and 3				
Control	2.89	2.44	2.16	2.43
New	2.58	1.81	1.97	2.13
Östergarnsholm between levels 5 and 4				
Control	3.54	2.29	2.32	2.71
New	2.87	1.76	1.94	2.21

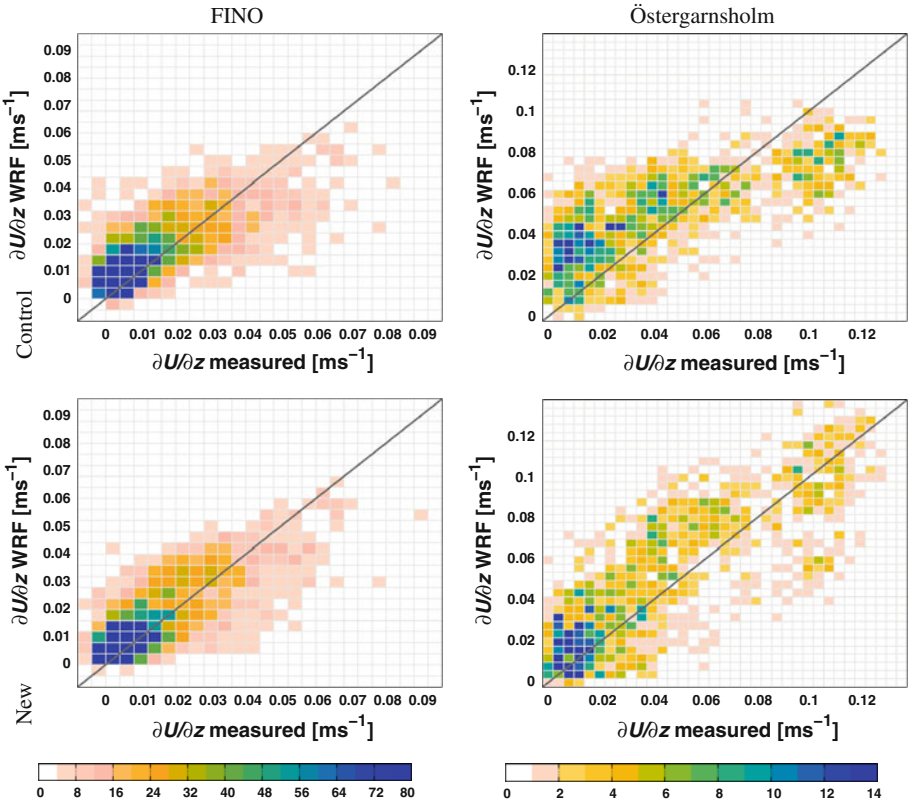

Fig. 10 Same as Fig. 7, only for wind-speed difference between 80 and 40 m at FINO and levels 5 and 4 at Östergarnsholm

difference between measurement levels, between the new parameterization compared to the control one.

5 Conclusions and Discussions

The WRF model (V 2.2) was used to downscale the wind field over the North Sea and the Baltic Sea for a high resolution representation of the structure of the lower part of the boundary layer (up to around 100 m above m.s.l.). A number of boundary-layer and surface-layer schemes are available in the WRF model; for example two schemes based on prescribed profiles of the turbulent exchange coefficients (i.e. K-theory) described in Hong and Pan (1996) and Hong et al. (2006) respectively, and the MYJ scheme (Janjić 2002) based on a prognostic equation for the TKE. The MJY scheme was chosen as the most promising, since the TKE-based schemes are expected to describe the boundary-layer physics more realistically and are in general more likely to reproduce realistic vertical profiles of wind and potential temperature compared to the K-theory schemes (e.g. Alapaty et al. 1997). The WRF simulated wind conditions were compared to the wind observations from the Östergarnsholm tower in the Baltic Sea (with wind-speed measurements up to around 30 m above m.s.l.) and

the FINO tower in the North Sea (with the measured wind conditions between 40 and 80 m above m.s.l.).

The simulated wind shear shows consistent deviations with respect to observations. In the stable (unstable) surface layer,[7] the simulated wind shear is consistently lower (higher) than observed. The differences between the simulations and observations are more pronounced close to the surface (Östergarnsholm) than higher in the boundary layer (FINO).

The parameterization of the surface layer and boundary layer was identified as the most probable reason for the inability of the WRF model to reproduce the observed wind shear. In order to improve the simulated wind shear, the MYJ surface-layer and boundary-layer parameterizations were modified by changing the MLS mainly following the approach described by Nakanishi (2001). The MLS controls the turbulent diffusion and dissipation, and the pressure–strain and pressure–temperature covariances. Many definitions of the MLS exist, some of which are cited in the Introduction. In the control (original) MYJ scheme, the Prandtl mixing length is used as the MLS in the surface layer and a combination of the Prandtl mixing length and the length based on the bulk turbulent property of the boundary layer is used as the MLS in the actual boundary layer (Mellor and Yamada 1982). The new surface-layer MLS is stability dependent and mimics the enhancement (suppression) of the mixing efficiency in the unstable (stable) surface layer. In the actual boundary layer, the new MLS is a combination of a stability adjusted Prandtl mixing length, a length scale based on the bulk turbulent property of the boundary layer and a length scale limiting the MLS due to the non-local surface forcing in the statically stable boundary layer. The high resolution wind measurements at FINO provided a means to estimate the surface length scale. We found evidence that the surface length scale is stability dependent and agrees well with that proposed by Nakanishi (2001).

Except close to the surface, the errors in the wind speed due to parameterizations are significantly lower compared to other errors, such as a poorly resolved mesoscale field used as initial and lateral boundary conditions in the WRF model. An improvement in the description of the mesoscale field is possible by the assimilation of observational data such as from nearby measurement stations (e.g. Ruggiero et al. 1996), or from satellite measurements: for example marine surface winds (Atlas et al. 2001).

The change of the surface-layer and boundary-layer parameterizations presented here was relatively simple in terms of modifying the WRF code. The introduction of the higher order MJY scheme (e.g. Nakanishi 2001) in the boundary layer by including new terms would represent the boundary-layer physics in more detail and thus possibly predict the wind profiles better. On the other hand, simpler adjustments of the original MJY scheme by varying the values of the parameters B_1 and S_q controlling the rate of the diffusion and dissipation of the TKE in (Eq. 24), as well as α in the definition of the MLS (Eq. 2), was not successful. We were not able to obtain the stability dependent corrections of the wind shear since by improving the wind shear in the case of the stable (unstable) layer, the wind shear in unstable (stable) conditions was worsened.

The new parameterization yields considerably different wind shears from the control case in the first few tens of metres, while higher in the boundary layer, the difference is smaller. In the new parameterization, the near-surface wind shears are generally larger in the stable surface layer and smaller in the unstable surface layer. The wind shear from the new parameterization shows considerably closer agreement with the observations close to the surface (up to around 30 m, at Östergarnsholm). Higher in the boundary layer (between 40 and 80 m, at FINO), the improvements are less evident. However, at the FINO measurement levels, the wind shear is usually smaller and thus the measured wind shear is more prone to

[7] Surface stability was characterized by the inverse Obukhov length ($1/L$).

measurement errors than closer to the surface. The profiles of potential temperature change in a similar manner as the profiles of the wind speed, i.e. in the stable surface layer, the near-surface gradients of the potential temperature are higher than in the unstable layer. We have not presented the change of the potential temperature profiles between the control and new parameterization due to the lack of reliable temperature profile measurements.

It was observed that the new parameterization, as well as the control one, is very sensitive to the correct specification of the lower boundary condition for the surface layer. The new parameterization is even more sensitive to the surface stability than the original since it is explicitly used in the definition of the MLS. The new boundary-layer parameterization was tested in the marine PBL since the lower boundary condition is relatively homogeneous compared to land where even small undulations of the terrain and vegetation heterogeneity complicate the interaction between land and atmosphere. However, in case of the marine PBL, the dynamical interaction between the sea and the atmosphere must be taken into account, which mainly influences the momentum transfer between the sea and atmosphere. In the current version of the WRF model, the momentum forcing from the sea to the atmosphere is described by the simple Charnock relationship. There is evidence that the coupling of the wave model to the atmospheric model is required to describe the dynamical coupling of the atmosphere to the ocean that potentially also improves the low-level wind simulations (Desjardins et al. 2000). The heat forcing is dependent on the accurate specification of SST and diffusion layer parameterization, and it was found that over the Baltic Sea a relatively high spatially resolved SST was required to properly describe surface heat forcing. The other uncertainty of the WRF simulation result includes a proper description of the moist processes that can have an important influence on the structure of the boundary layer (Stevens 2005), especially at the measurement locations where the boundary layer over the North Sea and Baltic Sea is often capped by clouds. Future work will consider the description of the influence of the moist processes on boundary-layer structure in more detail.

Acknowledgements The work shown here was supported by the EU program Marie-Curie, Early Stage Researcher Program Modobs (MRTN-CT-2005-019369) and OWEA project supported by German Federal Ministry for Environment, Nature conservation and Nuclear Safety. The tower measurement data were provided by the University of Uppsala and German Wind Energy Institute, the SST in the Baltic Sea by German Federal Maritime and Hydrographic Agency and the FNL data by US National Centers for Environmental Prediction. We are also grateful to the developers of WRF for providing the model for public use. We thank A. Rutgersson for useful comments on the manuscript and preparing the Östergarnsholm observational dataset used in this study. We would also like to thank three anonymous reviewers who helped improve the manuscript.

Appendix A: MYJ equations in WRF model

The equations of the MYJ level-2.5 and level-2 model are presented; more details can be found in Mellor and Yamada (1974, 1982) and Janjić (2002). The boundary-layer parameterization estimates turbulent exchange coefficients for momentum (K_M) and heat (K_H):

$$\overline{u_i' w'} = -K_M \frac{\partial u_i}{\partial z}, \tag{16}$$

where $i = 1, 2$

$$\overline{w' \theta_v'} = -K_H \frac{\partial \theta_v}{\partial z}. \tag{17}$$

For moisture and other passive tracers, K_H is used as the relevant exchange coefficient. The following non-dimensional variables are defined: wind shear (G_M), vertical gradient of

virtual potential temperature (G_H), diffusion coefficients for momentum and heat (S_M and S_H, respectively):

$$G_M = \frac{l^2}{q^2}\left(\left(\frac{\partial U}{\partial z}\right)^2 + \left(\frac{\partial V}{\partial z}\right)^2\right), \tag{18}$$

$$G_H = -\frac{l^2}{q^2}\beta g \frac{\partial \theta_v}{\partial z}, \tag{19}$$

$$S_M = -\frac{\overline{w'u_i'}}{lq\frac{\partial U_i}{\partial z}}, \tag{20}$$

$$S_H = -\frac{\overline{w'\theta_v'}}{lq\frac{\partial \theta_v}{\partial z}}, \tag{21}$$

where l is the MLS and $\frac{1}{2}q^2$ is the TKE. The MYJ level-2.5 model can be written with two algebraic equations relating the non-dimensional wind shear and vertical gradient of potential temperature and prognostic equation for TKE:

$$S_M(6A_1A_2G_M) + S_H(1 - 3A_2B_2G_H - 12A_1A_2G_H) = A_2, \tag{22}$$

$$S_M(1 + 6A_1^2G_M - 9A_1A_2G_H) - S_H(12A_1^2G_H + 9A_1A_2G_H) = A_1(1 - 3C_1), \tag{23}$$

$$\frac{1}{2}\frac{\partial q^2}{\partial t} + U_i\frac{\partial q^2}{2\partial x_i} = \frac{\partial}{\partial z}\left(lqS_q\frac{\partial q^2}{2\partial z}\right) = -\overline{w'u'}\frac{\partial U}{\partial z} - \overline{w'v'}\frac{\partial V}{\partial z} + \beta g\overline{\theta_v'w'} - \frac{q^3}{B_1 l}. \tag{24}$$

The values of the parameters A_1, A_2, B_1, B_2, C_1 and S_q are obtained empirically and given in Janjić (2002). The turbulent exchange coefficients (K_M and K_H) and consequently the turbulent fluxes can be calculated from Eqs. 22–24, using the definitions of the non-dimensional vertical gradients. The MYJ level-2.5 scheme is known to be numerically unstable in the cases of rapidly growing or rapidly decaying turbulence due to the assumptions of near-isotropy for the turbulent fluxes (e.g. Helfland and Labraga, 1988). Janjić (2002) solved the numerical instability of the scheme by imposing an upper limit to the MLS, which is a function of the local TKE.

The MYJ level-2 model is obtained by assuming local equilibrium between the production and dissipation of TKE. With this assumption the prognostic equation for TKE simplifies to the algebraic equation, and mixing coefficients can be written as a function of flux Richardson number, defined as:

$$R_f = \frac{\frac{g}{\theta_v}\overline{\theta_v'w'}}{\overline{u'w'}\frac{\partial U}{\partial z} + \overline{v'w'}\frac{\partial V}{\partial z}}. \tag{25}$$

The non-dimensional diffusion coefficients for momentum and heat are expressed as:

$$S_M = 3A_1\frac{\gamma_1 - C_1 - (6A_1 + 3A_2)\Gamma/B_1}{\gamma_1 - \gamma_2\Gamma + 3A_1\Gamma/B_1}(\gamma_1 - \gamma_2\Gamma), \tag{26}$$

$$S_H = 3A_2(\gamma_1 - \gamma_2\Gamma) \tag{27}$$

where the new stability function (Γ) and the constants (γ_1 and γ_2) are:

$$\Gamma = \frac{R_f}{1 - R_f}, \tag{28}$$

$$\gamma_1 = \frac{1}{3} - \frac{2A_1}{B_1}, \tag{29}$$

$$\gamma_2 = \frac{B_2 + 6A_1}{B_1}. \tag{30}$$

Over the sea the atmospheric surface layer is linked to the surface through a thin diffusive layer (Liu et al. 1979; Janjić 1994). The diffusive layer exists only when the friction velocity is small enough, i.e. the sea is smooth. The SST is prescribed as the boundary condition and is kept constant through the simulation period. The roughness length is calculated using the Charnock relationship (Janjić 1994) based on the friction velocity.

References

Alapaty K, Pleim JE, Raman S, Niyogi DS, Byun DW (1997) Simulation of atmospheric boundary layer processes using local- and nonlocal-closure schemes. J Appl Meteorol 36(3):214–233

Atlas R et al (2001) The effects of marine winds from scatterometer data on weather analysis and forecasting. Bull Am Meteorol Soc 82(9):1965–1990

Canuto VM, Cheng Y, Howard A (2001) New third-order moments for the convective boundary layer. J Atmos Sci 58(9):1169–1172

Chen F, Janjić Z, Mitchell K (1997) Impact of atmospheric surface-layer parameterizations in the new land-surface scheme of the NCEP mesoscale ETA model. Boundary-Layer Meteorol 85(3):391–421

Cheng Y, Canuto VM, Howard AM (2002) An improved model for the turbulent PBL. J Atmos Sci 59(9):1550–1565

Desjardins S, Mailhot J, Lalbeharry R (2000) Examination of the impact of a coupled atmospheric and ocean wave system. Part I: atmospheric aspects. J Phys Oceanogr 30(2):385–401

Gryning S-E, Batchvarova E, Brümmer B, Jørgensen H, Larsen S (2007) On the extension of the wind profile over homogeneous terrain beyond the surface boundary layer. Boundary-Layer Meteorol 124(2):251–268

Helfland HM, Labraga JC (1988) Design of a nonsingular level 2.5 second-order closure model for the prediction of atmospheric turbulence. J Atmos Sci 45(2):113–132

Holtslag AAM, de Bruin HAR (1988) Applied modeling of the nighttime surface energy balance over land. J Appl Meteorol 27(6):689–704

Hong S-Y, Pan H-L (1996) Nonlocal boundary layer vertical diffusion in a Medium-Range Forecast model. Mon Weather Rev 124(10):2322–2339

Hong S-Y, Noh Y, Dudhia J (2006) A new vertical diffusion package with an explicit treatment of entrainment processes. Mon Weather Rev 134(9):2318–2341

Iwata H, Asanuma J, Ohtani Y, Mizoguchi Y, Yasuda Y (2009) Vertical length scale of transporting eddies for sensible heat in the unstable roughness sublayer over a forest canopy. J Agric Meteorol 65(1):1–9

Janjić Z (1994) The step-mountain ETA coordinate model: further development of the convection, viscous sublayer and turbulence closure scheme. Mon Weather Rev 122(5):927–945

Janjić Z (2002) Nonsingular implementation of the Mellor–Yamada level 2.5 scheme in the NCEP meso model. NCEP Office Note No. 437, 60

Lenderink G, Holtslag AAM (2004) An updated length-scale formulation for turbulent mixing in clear and cloudy boundary layers. Q J Roy Meteorol Soc 130(604):3405–3427

Liu WT, Katsaros KB, Businger JA (1979) Bulk parameterization of air–sea exchanges of heat and water vapor including the molecular constraints at the interface. J Atmos Sci 36(9):1722–1734

Łobocki L (1992) Mellor–Yamada simplified second-order closure models: analysis and application of the generalized von Karman local similarity hypothesis. Boundary-Layer Meteorol 59(1–2):83–109

Łobocki L (1993) A procedure for the derivation of surface-layer bulk relationship from simplified second-order closure models. J Appl Meteorol 32(1):126–138

Mellor GL, Yamada T (1974) A hierarchy of turbulence closure models for planetary boundary layers. J Atmos Sci 31(7):1791–1806

Mellor GL, Yamada T (1982) Development of a turbulence closure model for geophysical fluid problems. Rev Geophys Space Phys 20(4):851–875
Moeng C, Wyngaard JC (1989) Evaluation of turbulent transport and dissipation closures in second-order modeling. J Atmos Sci 46(14):2311–2330
Nakanishi M (2001) Improvement of the Mellor–Yamada turbulence closure model based on large-eddy simulation data. Boundary-Layer Meteorol 99(3):349–378
Neumann T, Nolopp K, Herklotz K (2004) First operating experience with the FINO1 research platform in the North Sea. DEWI Magazine 24:27–34
Rotta J (1951) Statistische theorie nichthomogener Turbulenz. Z Phys 129:547–572
Ruggiero FH, Sashegyi KD, Madala RV, Raman S (1996) The use of the surface observations in four-dimensional data assimilation using a mesoscale model. Mon Weather Rev 124(5):1018–1033
Rutgersson A, Smedman A-S, Högström (2001) Use of a conventional stability during swell. J Geophys Res 27(134):117–134
Sjöblom A, Smedman A-S (2003) Vertical structure in the marine atmospheric boundary layer and its application for the inertial disspiation method. Boundary-Layer Meteorol 109(1):1–25
Skamarock WC, Klemp JB, Dudhia J, Gill DO, Barker DM, Wang W, Powers JG (2005) A description of the advanced research wrf version 2. Tech. rep., NCEP/NCAR, 88 pp. http://www.mmm.ucar.edu/wrf/users/docs/arw_v2.pdf
Smedman A-S, Högström U, Bergström H, Rutgersson A, Kahma K, Pettersson H (1999) A case study of air–sea interaction during swell conditions. J Geophys Res 25(104):25833–25851
Stevens B (2005) Atmospheric moist convection. Annu Rev Earth Planet Sci 33:605–643
Stull RB (1988) An introduction to boundary layer meteorology. Kluwer, Dordrecht, 666 pp
Sušelj K (2009) Modeling of the near surface wind speed: Boundary layer and climate aspects. PhD thesis, University of Oldenburg, 135 pp
Teixeira J, Cheinet S (2004) A simple mixing length formulation for the eddy-diffusivity parameterization of dry convection. Boundary-Layer Meteorol 110(3):435–453
Teixeira J, Ferreira JP, Miranda P, Haack T, Doyle J, Siebesma AP, Salgado R (2004) A new mixing length formulation for the parameterization of dry convection: implementation and evaluation in a mesoscale model. Mon Weather Rev 132(11):2698–2707
Therry G, Lacarrére P (1983) Improving the eddy kinetic energy model for planetary boundary layer description. J Atmos Sci 25(1):63–88
Umlauf L, Burchard H (2003) A generic length-scale for geophysical turbulence models. J Mar Res 61(2):235–265
Vickers D, Mahrt L (1997) Quality control and flux sampling for tower and aircraft data. J Atmos Oceanic Technol 14(3):512–526
Wilczak JM, Oncley SP, Stage SA (2001) Sonic anemometer tilt correction algorithms. Boundary-Layer Meteorol 99(1):127–150